Received: 8 October 2022 | Accepted: 6 December 2022

DOI: 10.1002/pamm.202200291

Image-based analysis of complex microstructures using the finite cell method

Mahan Gorji[1,*], **Michail Komodromos**[2], **Jürgen Grabe**[2], and **Alexander Düster**[1]

[1] Hamburg University of Technology, Numerical Structural Analysis with Application in Ship Technology (M-10), Am Schwarzenberg-Campus 4 (C), 21073 Hamburg

[2] Hamburg University of Technology, Institute of Geotechnical Engineering and Construction Management (B-5), Harburger Schloßstraße 36, 21079 Hamburg

Geometry conforming meshing techniques such as the finite element method (FEM) face a big challenge when dealing with complex and heterogeneous microstructures. Therefore, efficient simulation methods are needed combining accurate morphological reproducibility and computational efficiency. For such problems, the finite cell method (FCM) is a promising approach, which uses a Cartesian grid – independent of the geometry – leading to a fast and efficient mesh generation. However, to handle complex microstructures such as cemented sands the FCM is not sufficient anymore. Therefore, three different versions of the FCM are presented: first, the FCM, which is directly applied to CT scans (denoted as "VoxelFCM"). Second, the FCM combined with a global L^2-projection, leading to a smooth geometry description (denoted as "FCM"). And finally, the FCM with L^2-projection, which is extended by a local enrichment to capture weak discontinuities at the interfaces between the different phases (denoted as "FCM-Enrichment"). First, in a numerical study, the different versions of the FCM are investigated. Then, these methods are verified against the FEM. Finally, these methods are used to gain a deeper insight into the micromechanical phenomena of cemented sands under compressive loading.

1 Introduction

The finite element method (FEM) is a well-known numerical tool for solving problems in structural mechanics. The FEM uses a geometry conforming mesh to discretize the structure. For most geometries this technique can be very efficient. However, when dealing with complex microstructures - such as cemented sand, as shown in Fig. 1 (a) - the FEM would need a very fine mesh to accurately resolve all the details of the highly irregular morphology of the cemented sand, leading to a large number of degrees of freedom.

In addition, the cemented sand shown in Fig. 1 (a) cannot be discretized directly, but rather a model for the geometry is needed first. Here, the geometry will be described by means of computer tomography (CT) scans, on which image processing is applied first and finally, the CT images are segmented using thresholding. In particular, the image processing is done by applying filters on the histogram of the CT image. Here, the histogram is aligned first in axial and then, in radial direction. Finally, shining artefacts are removed by a cutoff filter. The output is shown in Fig. 1 (b), where the different phases such as cement matrix, grain particles and void pores can be seen. Also, to distinguish between the different phases, special treatment is needed in the meshing process.

To overcome these issues, the finite cell method (FCM) as an alternative discretization technique is utilized. In particular, three different versions of the FCM are presented and applied to problems with image-based geometries (CT scans). The performance of the proposed methods is investigated by a numerical example of cemented sand, considering only a 2D subset of the CT scan, as shown in Fig. 1 (c) and thus, significantly simplifying the problem.

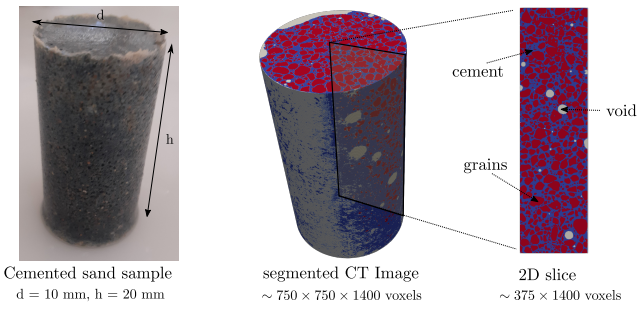

Fig. 1: (a) Cemented sand with diameter d and height h. (b) Image-processed and segmented CT scan. (c) Subset of CT scan.

* Corresponding author: e-mail mahan.gorji@tuhh.de, phone +49 40 42878 6099

2 Fast and efficient discretization using the finite cell method

2.1 Finite cell method

In the first step, the FCM is considered without any extensions. The FCM combines high-order finite elements with the fictitious domain approach [1], by which arbitrary complex geometries can be meshed directly into a Cartesian grid and thus, leading to a fast and simple meshing procedure. The FCM works on different geometry models such as implicit geometry representations (by level-set functions), B-rep models and voxel models and constructive solid geometry [1, 2]. Emphasis is given to voxel models, which are directly obtained from CT scans. A simple 2D example is displayed in Fig. 2, where the voxel model is directly meshed by the FCM. In this example, the mesh consists of 2×2 finite cells. If the CT scan was already segmented, the different phases could be directly obtained by the corresponding gray scale values of the voxels. For raw CT scans, the segmentation can also be done during the FCM computation.

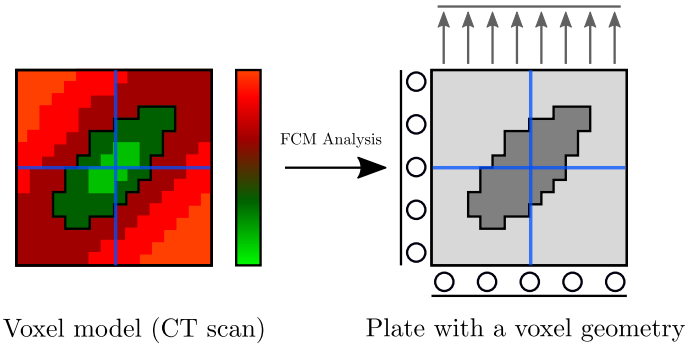

Fig. 2: FCM applied to a CT scan.

2.2 Finite cell method with L^2-projection

Applying the FCM directly to the voxel model leads to a non-smooth geometry description, which can cause singularities in the stresses and thus, adversely affect the accuracy [3, 4]. Therefore, the FCM is extended by a global L^2-projection. The idea, shown in Fig. 3, is to compute a smooth level-set function from the voxel model [3], which is then used as an implicit geometry description for the FCM. For the level-set function the following approximation is used:

$$\tilde{\phi}(\mathbf{x}) = \sum_{i=1}^{n} N_i(\mathbf{x})\, a_i \,. \tag{1}$$

Here, N_i are hierarchical shape functions (integrated Legendre polynomials) [5] and a_i the unknown coefficients. This ansatz minimizes a least-squares problem, which means that the level-set function represents the voxel model [2]. First, local system matrices and right-hand sides are computed for each finite cell and assembled into a global system of equations, which is then finally solved [4].

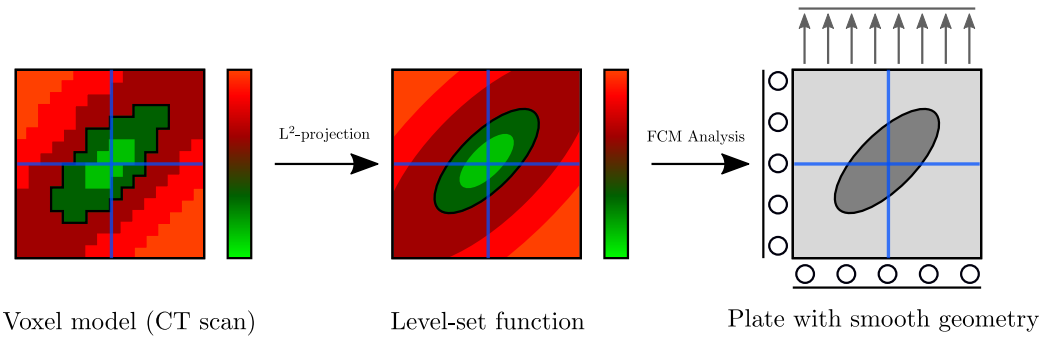

Fig. 3: FCM combined with a L^2-projection and applied to a CT scan.

2.3 Finite cell method with L^2-projection and local enrichment

In heterogeneous problems weak discontinuities occur at the interfaces between the different phases. These discontinuities correspond to kinks in the displacements and jumps in the strains and stresses. Since the FCM uses only smooth polynomials, it is not possible to capture the discontinuous part of the solution accurately and therefore, the convergence rate deteriorates.

To overcome this issue, the FCM is extended by a local enrichment, which is based on the hp-d method combined with a high-order partition of unity (PUM) approach [6]. With this approach, the discontinuities in the heterogeneous materials can be captured very precisely by a smooth level-set function, which in this work is directly obtained by the L^2-projection.

3 Numerical example

The different versions of the FCM are applied to cemented sand under compressive loading. For the sake of simplicity, a 2D slice of the CT scan of the cemented sand with 375 × 1350 voxels and a voxel size of 13 µm is considered, which reduces the spatial dimension of the problem by one accelerating the solution process. In this work, the fact that the morphology of the real 3D structure is not homogeneous for different slices (under rotation along the vertical axis by different angles) is neglected, see Fig. 1 (b) - (c). However, still meaningful results can be obtained, if the problem is modeled in 2D using axisymmetric elements and proper boundary conditions are chosen, which can represent the radial expansion and axial compression of the 3D cylinder. On the top boundary, a prescribed compression with a displacement of $\overline{u}_z = 1\,\mu\text{m}$ in axial direction is applied. A linear elastic material behaviour is assumed with a Young's modulus of $E_{\text{cement}} = 30\,\text{MPa}$ and a Poisson's ratio of $\nu_{\text{cement}} = 0.2$ for the cement matrix. Respectively, a Young's modulus of $E_{\text{grain}} = 1000 \cdot E_{\text{cement}}$ and a Poisson's ratio of $\nu_{\text{grain}} = 0.01$ for the grain particles are assumed. The voids are treated as a fictitious domain with $\alpha_{\text{FCM}} = E_{\text{void}}/E_{\text{cement}} = 10^{-6}$. The morphology, loads and boundary conditions as well as a cutline (green color) are shown in Fig. 4 (a). For all versions of the FCM as well as for the L^2-projection, the mesh is defined by the number of finite cells in every direction. The number of finite cells is defined by the number of voxels per finite cell (NVC), which is the same for all directions [7]. Different meshes are shown in Fig. 4 (b) - (d).

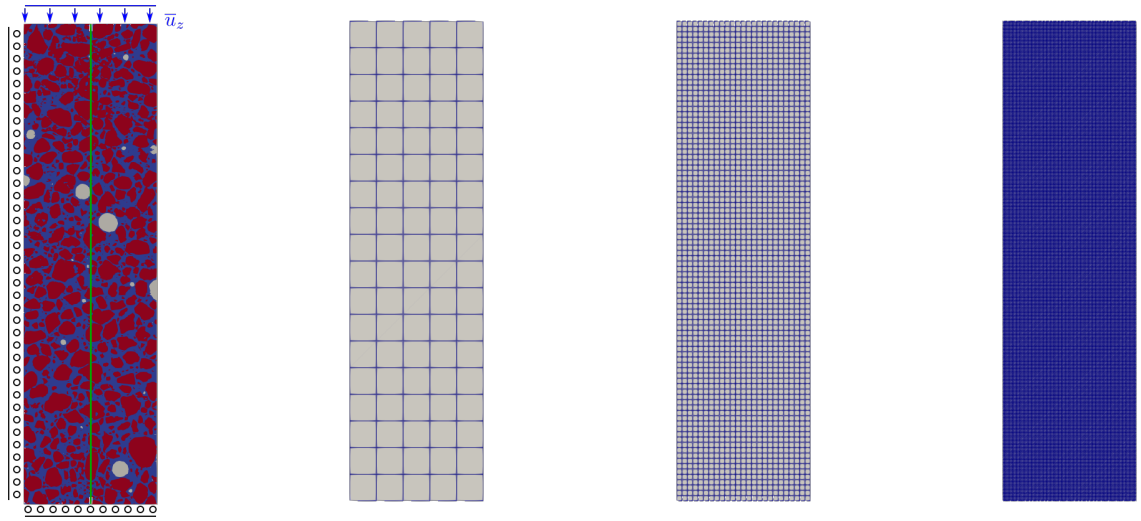

(a) Setup **(b)** NVC = 75 **(c)** NVC = 15 **(d)** NVC = 3

Fig. 4: (a) Setup of the problem. (b) - (d) Meshes for different NVC. A smaller NVC leads to a finer mesh.

3.1 Performance study of the different versions of the FCM

At first, the performance of the different versions of the FCM is studied for different meshes with $\text{NVC} \in \{3, 5, 15, 25, 75\}$. Here, the polynomial order p of the FCM ansatz is increased from 1 to 8, while the polynomial order of the L^2-projection is kept fix ($p^{\text{LS}} = 4$). For the enrichment, the ansatz is the same as the base ansatz ($p_e = p$), while the ansatz of the enrichment function is the same as the one for the L^2-projection ($p_F = p^{\text{LS}}$). For the numerical integration, a quad-tree with a tree-depth of $\mathcal{R} = 3$ and $n_G = p^* + 1$ Gauss points in each direction is used, where $p^* = \max\{p,\, p_e + p_F\} = p + 4$ if enrichment is applied and otherwise, $p^* = p$. The results are shown in Fig. 5 (a), where the strain energy is plotted against the number of degrees of freedom n_{dof} of the FCM ansatz. From this it is evident that for all versions of the FCM convergence is achieved. The convergence behaviour is similar between the different versions, but the L^2-projection slightly improves the accuracy. To get more insight, the relative error in strain energy

$$e_r = \left| \frac{\mathcal{U}^{\text{FCM}} - \mathcal{U}^{\text{ref}}}{\mathcal{U}^{\text{ref}}} \right| \tag{2}$$

is displayed in Fig. 5 (b), where the reference strain energy $\mathcal{U}_{\text{ref}} = 3.441785134927812 \cdot 10^{-4}$ is obtained from an overkill solution using the FCM directly applied to the voxel model. Here, every voxel is discretized by one finite cell (NVC = 1)

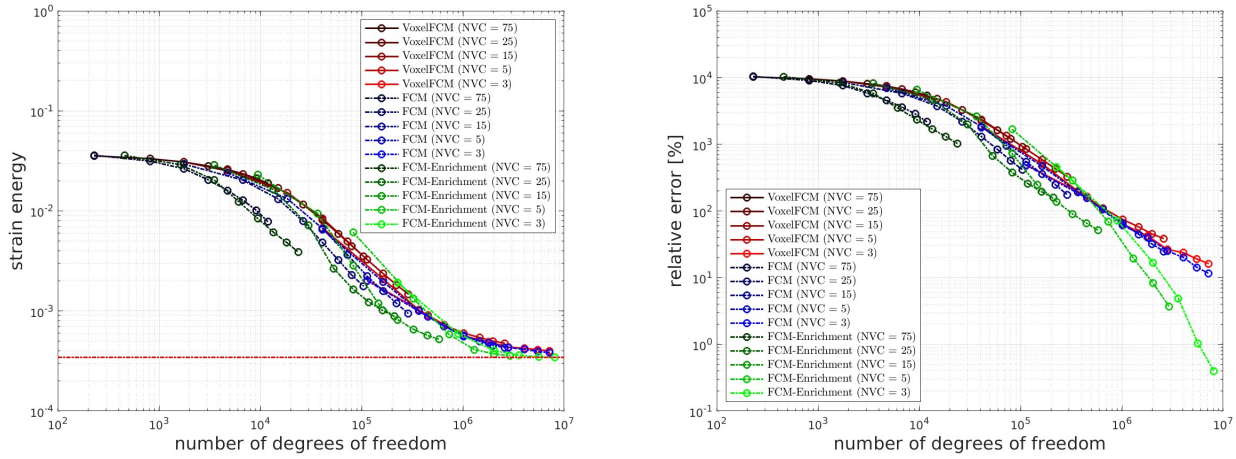

(a) Strain energy **(b)** Relative error in strain energy

Fig. 5: Convergence study for $p = 1, 2, \ldots, 8$. (a) Strain energy. (b) Relative error in strain energy norm.

and high-order shape functions of order $p = 4$ are employed. It can be seen that the enrichment improves the results, where a relative error below 1 % can be achieved.

3.2 Verification with FEM

The next step is the verification of the different versions of the FCM by comparing them with the FEM. For the FEM, an image-adapted algorithm was applied, which reads the voxel model and discretizes the different phases with a geometry conforming mesh using triangular elements. The FEM mesh is then imported into the commercial finite element software ABAQUS [8], where the mechanical problem is finally solved. The FEM results serve as a reference solution.

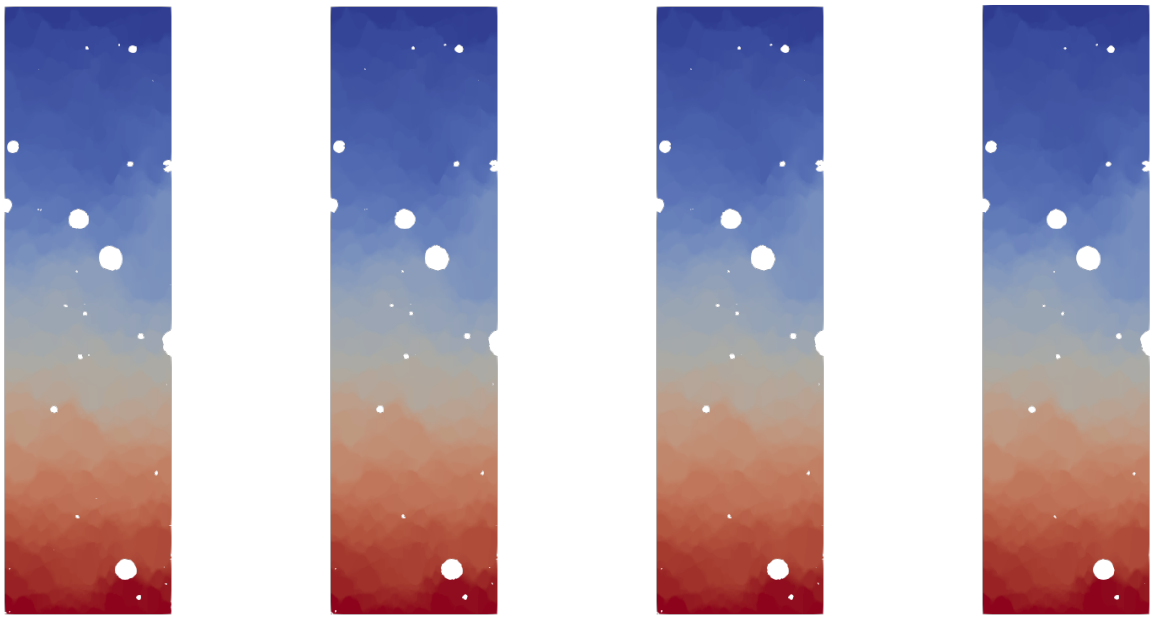

(a) VoxelFCM $(\mathbf{NVC = 3, p = 8})$ **(b) FCM** $(\mathbf{NVC = 3, p = 8})$ **(c) FCM-Enrichment** $(\mathbf{NVC = 3, p = 6})$ **(d) FEM (reference)**

Fig. 6: Vertical displacement u_z. Comparison of the different versions of the FCM (a) - (c) with the FEM (d).

First, the vertical displacement u_z is compared between the different versions of the FCM and the FEM, as shown in a contour plot in Fig. 6. It is observed that all versions of the FCM show a good agreement with the FEM results. Next, the von Mises stress σ_{vM} is examined, as shown in Fig. 7. For the FCM without any L^2-projection (denoted as "VoxelFCM" in

Fig. 7 (a)), there are high stress concentrations around the interfaces between the cement matrix and grain particles. These concentrations are reduced, if the L^2-projection (denoted as "FCM" in Fig. 7 (b)) is applied and even further reduced, if the enrichment (denoted as "FCM-Enrichment" in Fig. 7 (c)) is used. This demonstrates that utilizing L^2-projection as well as enrichment to the FCM, the results can be clearly improved.

In addition, the vertical displacement u_z along a vertical cutline shown in Fig. 4 (a) is studied to provide a quantitative comparison. Similar to Fig. 6, the different versions of the FCM are very close to the reference solution provided by the FEM.

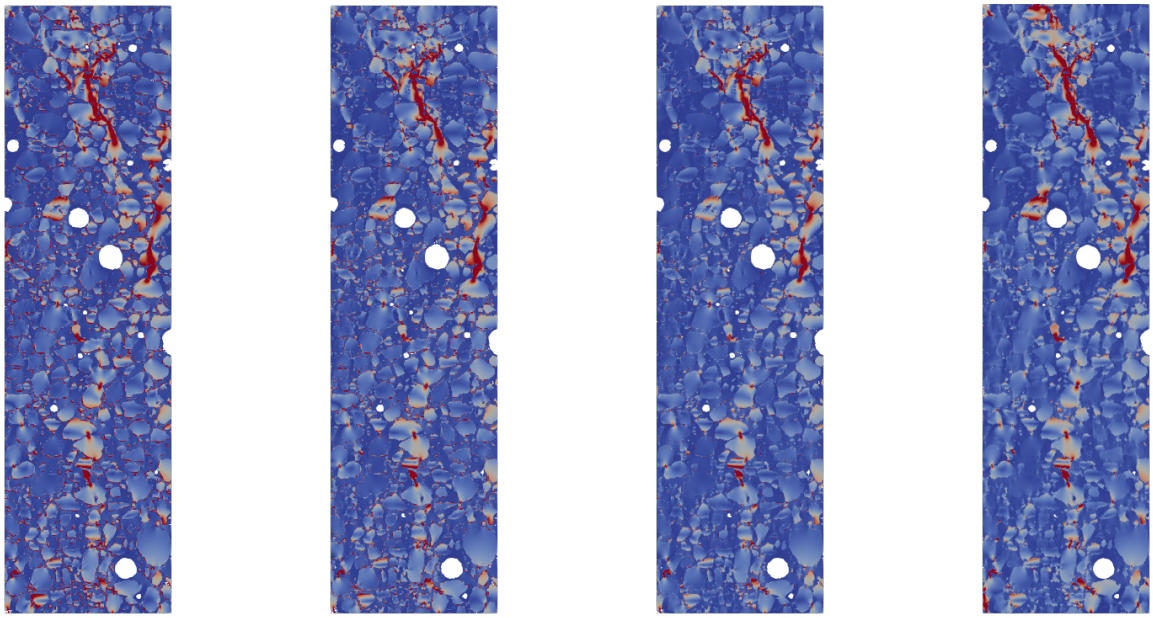

(a) VoxelFCM ($\mathbf{NVC = 3, p = 8}$) | **(b) FCM** ($\mathbf{NVC = 3, p = 8}$) | **(c) FCM-Enrichment** ($\mathbf{NVC = 3, p = 6}$) | **(d) FEM (reference)**

Fig. 7: von Mises stress σ_{vM}. Comparison of the different versions of the FCM (a) - (c) with the FEM (d).

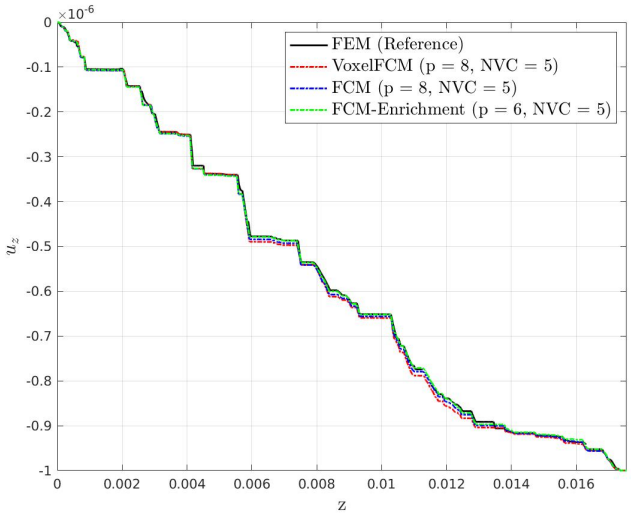

Fig. 8: Vertical displacement u_z along the cutline (shown in Fig. 4 (a)). Comparison of the different versions of the FCM with FEM.

4 Interpretation of the results

Finally, the proposed methods can be used to interpret the micromechanical effects of the cemented sand. Again, the cemented sand under compressive loading is considered with the same setup as in the previous section. To understand the trigerring

mechanisms of damage phenomena such as grain crushing and matrix cracking [9, 10], the von Mises stress σ_{vM} as an important failure indicator is examined. To compute the von Mises stress, the FCM with L^2-projection and enrichment (denoted as "FCM-Enrichment") is utilized with $\mathrm{NVC} = 3$ and $p = 6$.

In Fig. 9, the von Mises stress is visualized for the different phases. In Fig. 9 (a) high stress concentrations inside the grain particles can be observed, possibly leading the particles to break (grain crushing). Moreover, the high stress concentrations in the cement matrix in Fig. 9 (b) are probably caused by the movement of the grain particles, potentially leading the cement matrix to fail (matrix cracking). With the proposed method, the mechanisms triggering failure can be predicted and thus, a deeper insight into the micromechanical effects in cemented sands can be obtained.

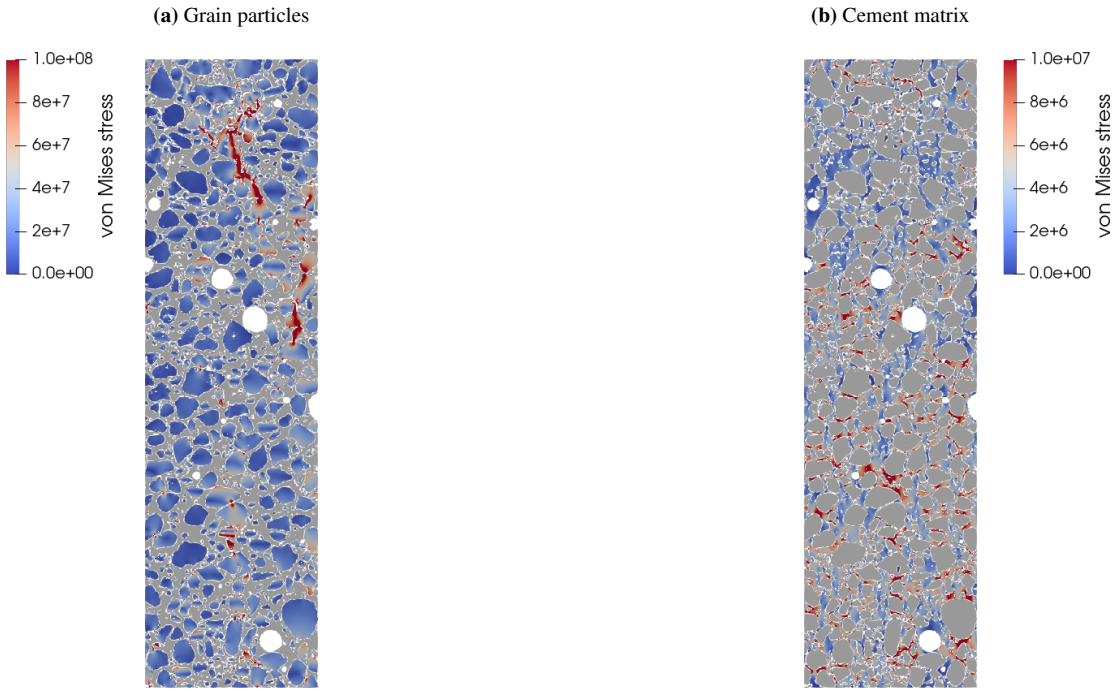

Fig. 9: von Mises stress σ_{vM} of the grain particles (a) and the cement matrix (b). Stress concentrations triggering grain crushing (a) and matrix cracking (b).

5 Conclusion

In this contribution different versions of the FCM were presented and applied to cemented sands under compressive loading. In a performance study, it was first demonstrated that extending the FCM by a L^2-projection and local enrichment, the results can be significantly improved. In addition, all versions of the FCM were verified against the FEM. Finally, the interpretation of results revealed that the proposed methods have the potential to study micromechanical phenomena.

Acknowledgements The authors gratefully acknowledge the support provided by the DFG (Deutsche Forschungsgemeinschaft) under the grant numbers GR 1024/41-1 and DU 405/17-1. Open access funding enabled and organized by Projekt DEAL.

References

[1] A. Düster, J. Parvizian, Z. Yang and E. Rank, Comput. Method. Appl. M. **197**, 3768–3782 (2008).
[2] B. Wassermann, S. Kollmannsberger, T. Bog and E. Rank, Comput. Math. Appl. **74**, 1703–1726 (2017).
[3] C.V. Verhoosel, G.J. van Zwieten, B. van Rietbergen and R. de Borst, Comput. Methods Appl. Mech. Engrg. **284**, 138–164 (2015).
[4] D. Schillinger, P.K. Ruthala and L.H. Nguyen, Int. J. Numer. Meth. Engng. **108**, 515–534 (2016).
[5] B.A. Szabó and I. Babuška, Finite Element Analysis (John Wiley & Sons, 1991).
[6] M. Joulaian and A. Düster, Comput. Mech. **52**, 741–762 (2013).
[7] S. Heinze, M. Joulaian and A. Düster, Comput. Math. Appl. **70**, 1501–1517 (2015).
[8] M. Smith, ABAQUS/Standard User's Manual, Version 6.9. United States: Dassault Systèmes Simulia Corp. (2009).
[9] A. Tengattini, A. Das, G.D. Nguyen, G. Viggiani, S.A. Hall and I. Einav, J. Mech. Phys. Solids **70**, 281–296 (2014).
[10] A. Das, A. Tengattini, G.D. Nguyen, G. Viggiani, S.A. Hall and I. Einav, J. Mech. Phys. Solids **70**, 382–405 (2014).